Available online at www.sciencedirect.com
ScienceDirect
International Journal of Heat and Mass Transfer 50 (2007) 4600–4606
International Journal of HEAT and MASS TRANSFER
www.elsevier.com/locate/ijhmt

Theoretical and experimental studies on laser transformation hardening of steel by customized beam

Michael K.H. Leung [a,*], H.C. Man [b], J.K. Yu [c]

[a] Department of Mechanical Engineering, The University of Hong Kong, Hong Kong, China
[b] Department of Industrial and Systems Engineering, The Hong Kong Polytechnic University, Hong Kong, China
[c] Environmental Corrosion Center, Institute of Metal Research, Chinese Academy of Sciences, China

Received 27 November 2005; received in revised form 1 March 2007
Available online 23 May 2007

Abstract

An exact solution was developed for a quasi-steady-moving-interface heat transfer problem in laser transformation hardening by a beam customized to a flat-top rectangular shape. The absorption and release of the latent heat were taken into account. The solution provided the body temperature, heating rate, and subsequent cooling rate. Using the IT and CCT diagrams, the rapid austenitization and pearlitic/martensitic phase transformation were determined for prediction of the hardening effect. In the experimental study, a diffractive optical kinoform (DOK) was used to customize a conventional Gaussian laser spot beam to a flat-top rectangular beam. A reasonable agreement between the theoretical predictions and the experimental measurements was obtained.

Keywords: Laser transformation hardening; Flat-top rectangular beam; Moving phase-change interface; Exact solution

1. Introduction

Laser can be used for a wide range of surface heat treatment. A high power density laser operating at a slow traversing speed can cause the heated surface to melt. The surface can thus be treated for glazing, sealing, alloying, cladding, and material homogenization. On the other hand, a low power density laser operating at a fast traversing speed can be used for surface hardening. In this process, the cooling of the work area can be effected by rapid internal heat diffusion through the bulk material surrounding the heated region. An extrinsic quenching process is thus unnecessary.

In laser transformation hardening of steel, the material heated by a moving laser beam develops two phase-transformation interfaces moving along with the beam. The leading interface involves material heated above the austenitization temperature to change phase from cementite/ferrite mixture to austenite. The austensite is then rapidly cooled and transformed into pearlite or martensite at the trailing interface. As the interfaces absorb and release latent heat due to the phase transformations, the problem can be classified as a moving-interface heat transfer problem. The transient problem can be analyzed for the quasi-steady state that is applicable for modeling many continuous industrial production processes.

When the laser heat treatment is needed for a large surface area, the laser equipment can be set up to employ the automated overlapping method. Conventional overlapping with a Gaussian laser spot beam often results in adverse tempering effect and irregular surface hardness [1]. Alternatively, an ordinary spot beam can be customized to a longitudinal shape to alter the heat flux distribution resulting in a uniform surface treatment with less overlapped zone. It was found that a slope intensity profile could hold the heated zone in the austenitization temperature range longer so that the subsequent martensitic transformation would be more uniform within the case depth [2].

* Corresponding author. Tel.: +852 2859 2628; fax: +852 2858 5415.
E-mail address: mkhleung@hku.hk (M.K.H. Leung).

0017-9310/$ - see front matter © 2007 Elsevier Ltd. All rights reserved.
doi:10.1016/j.ijheatmasstransfer.2007.03.022

Nomenclature

Bi	Biot number
c	specific heat
C_n	coefficient in series and integral expansions
H	general eigenfunction
h	convective heat transfer coefficient
k	thermal conductivity
L	latent heat due to phase transformation
l_1''	x''-coordinate of leading-end of flat-top rectangular beam
l_2''	x''-coordinate of trailing-end of flat-top rectangular beam
N	normalization integral
n_j''	interface position
P	function defined in Eq. (27)
Pe	Pelect number
p_n	discrete eigenvalue
q	absorbed laser power
S_j''	x''-coordinate of interface
St	Stefan number
T	temperature
t	time
U	step function
u	thickness of specimen
V	feed rate
w	width of rectangular laser beam
x'', y''	fixed coordinates
x', y'	moving coordinates
x, y	dimensionless moving coordinates
Z	dimensionless temperature

Greek symbols

α	thermal diffusivity
δ	Dirac delta function
ρ	density
$v_{n,j}$	speed of moving interface in normal direction

Subscripts

0	lower surface
a	leading phase-transformation interface
b	trailing phase-transformation interface
p	phase change
u	upper surface

In the design of a beam profile for desirable hardening effect, theoretical modeling of the heat transfer and phase transformation can serve as a useful design tool. Komanduri and Hou [3] and Brockmann et al. [4] presented their analytical solutions to the heat transfer problem of a laser surface transformation hardening process in which a specimen was fed through a Gaussian laser beam. The absorption and release of the latent heat due to the moving phase-transformation interfaces were not considered in their works. The exact solutions of one-dimensional phase change due to a moving front were studied by Landau [5], Jackson [6], and Hsieh [7]. Hsieh derived another two-dimensional phase-change solution for a thin plate heated by a cylindrical moving heat front [8]. The solutions presented by Hsieh [7,8] utilized a source-and-sink method that has the virtue of deriving a single equation for the temperature distribution in all phase regions [9,10]. Based on the source-and-sink method, Hsieh and Leung [11] derived a solution that could simulate the heat transfer in progressive flame hardening of rotating shafts and bearings. Leung [12] also considered laser heat treatment by a moving Gaussian rectangular beam produced by oscillating mirrors.

In this research, the source-and-sink method was employed to derive a general solution for a customized laser beam. A flat-top rectangular beam, which could be produced by a diffractive optical kinoform (DOK) or a diode laser, was selected to illustrate the solution derivation. Experimental study on laser transformation hardening of AISI 1050 steel by DOK was conducted for validation of the theoretical solution. For the selected rectangular beam and feed rate tested, the surface of the steel sample was hardened due to transformation to pearlite instead of martensite. It was still justified to use the experimental data to validate the theoretical model developed in the present study because martensitic transformation and pearlitic transformation were of the same mechanisms.

2. Theoretical modeling

Fig. 1 illustrates a steel sample fed through a customized laser beam in a laser transformation hardening process. The customized laser beam has a uniform lengthwise intensity along the z' direction so as to minimize any adverse irregular hardening effect due to a Gaussian beam and

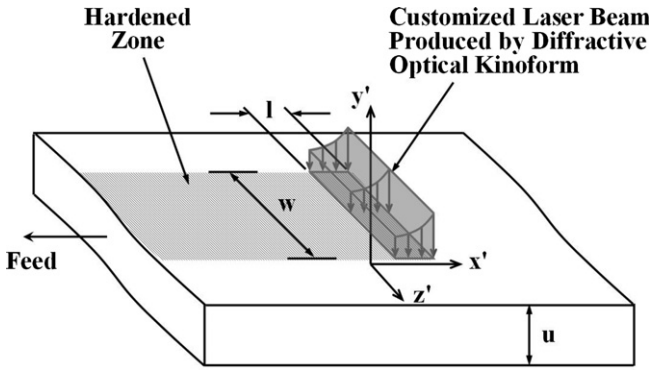

Fig. 1. Laser transformation hardening by customized beam.

substantial overlapping. The intensity profile along the x' direction can be manipulated in order to control the heating rate and cooling rate for proper phase transformation of the treated material. Since the base of the rectangular beam has a large length-to-width ratio, the heat transfer can be simulated by a two-dimensional model. This paper presents the derivation of theoretical solution for a laser beam customized to a flat-top, rectangular-base beam.

The setup shown in Fig. 1 can be represented by a stationary slab heated by a moving heat source at a constant velocity as illustrated in Fig. 2. The fixed coordinates and the moving coordinates are represented by (x'', y'') and (x', y'), respectively. It is assumed that the phase change is diffusion-driven in a medium of uniform properties in different phases. The assumption is justified as the phase transformation always involves in a solid state, which is entirely different from a solid–liquid phase change. The thermal properties (thermal conductivity, specific heat, etc.) in different phases, i.e. austenite, pearlite, ferrite, and martensite, do not vary considerably. The ratio of the beam length to width is large enough to neglect any lateral effects so that the problem domain becomes two-dimensional. The energy equation of this transient heat transfer problem can be expressed as

$$\nabla^2 T + \sum_{j=\mathrm{a,b}} \frac{\rho L_j}{k} v_{n,j} \delta(n'' - n''_j) = \frac{1}{\alpha}\frac{\partial T}{\partial t} \tag{1}$$

where the interfaces are situated at n''_j and moving at a velocity $v_{n,j}$ perpendicular to the interface. The interface movement in the normal direction can be presented in the x''-direction by using the following substitution as derived by Patel [13]

$$v_{n,j}\delta(n'' - n''_j) = \frac{\partial S''_j}{\partial t}\delta[x'' - S''_j(y'', t)], \quad j = \mathrm{a,b} \tag{2}$$

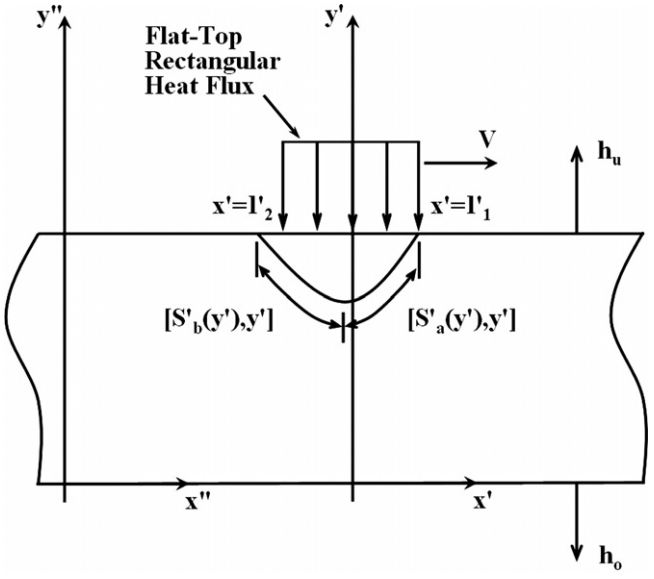

Fig. 2. Problem domain in fixed and moving two-dimensional coordinate systems.

and

$$T[S''_j(y'', t), y'', t] = T_\mathrm{p}, \quad j = \mathrm{a,b} \tag{3}$$

where $S''_j(y'', t)$ denotes the x''-coordinates of the interface positions and T_p is the phase-change temperature. The initial and the boundary conditions are given by

$$T(x'', y'', 0) = 0 < T_\mathrm{p} \tag{4}$$

$$\frac{\partial T(x'', u, t)}{\partial y''} + \frac{h_\mathrm{u}}{k} T(x'', u, t) = f(x'') \tag{5}$$

$$-\frac{\partial T(x'', 0, t)}{\partial y''} + \frac{h_0}{k} T(x'', 0, t) = 0 \tag{6}$$

$$T(-\infty, y'', t) = \begin{cases} \text{finite}, & h_\mathrm{u} = h_0 = 0 \\ 0, & h_\mathrm{u} > 0 \text{ or } h_0 > 0 \end{cases} \tag{7}$$

$$T(\infty, y'', t) = 0 \tag{8}$$

Eqs. (1)–(8) establish the general differential equation problem for the quasi-steady-moving-interface phenomena of laser transformation hardening. The derivation of the solution is illustrated for a specimen heated on top by a moving flat-top rectangular beam and insulated on bottom. The heat source represented by $f(x'')$ in Eq. (5) can be written as a composite of two step functions

$$f(x'') = \frac{q}{wk} \cdot \frac{U(x'' - Vt - l''_2) - U(x'' - Vt - l''_1)}{l''_1 - l''_2} \tag{9}$$

where q is the absorbed laser power; $U(z)$ is a step function with $U(z > 0) = 1$ and $U(z \leqslant 0) = 0$; l''_1 and l''_2 are the x''-coordinates of the leading-end and trailing-end of the rectangular beam, respectively. The insulation on the bottom surface implies that h_0 is zero. The transient problem can be converted to a dimensionless quasi-steady problem by the following substitutions:

$$x = \frac{x'' - Vt}{u}; \quad y = \frac{y''}{u}; \quad S_j = \frac{S'_j}{u}, \ j = \mathrm{a,b};$$
$$Z = \frac{wkT}{q}; \quad Z_\mathrm{p} = \frac{wkT_\mathrm{p}}{q}; \quad St_j = \frac{cT_\mathrm{p}}{L_j},$$
$$L_\mathrm{a} = -L_1, \ L_\mathrm{b} = L_2; \quad Pe = \frac{Vu}{\alpha}; \quad Bi_\mathrm{u} = \frac{h_\mathrm{u} u}{k} \tag{10a–h}$$

Accordingly, the governing equation, boundary conditions, and interface conditions can be written in the dimensionless form:

$$\nabla^2 Z + \sum_{j=\mathrm{a,b}} \frac{PeZ_\mathrm{p}}{St_j}\delta[x - S_j(y)] = -Pe\frac{\partial Z}{\partial x} \tag{11}$$

$$\frac{\partial Z(x, 1)}{\partial y} + Bi_\mathrm{u} Z(x, 1) = \frac{U(x - l_1) - U(x - l_2)}{l} \tag{12}$$

$$-\frac{\partial Z(x, 0)}{\partial y} = 0 \tag{13}$$

$$Z(-\infty, y) = \begin{cases} \text{finite}, & Bi_\mathrm{u} = 0 \\ 0, & Bi_\mathrm{u} > 0 \end{cases} \tag{14}$$

$$Z(\infty, y) = 0 \tag{15}$$

$$Z[S_j(y), y] = Z_\mathrm{p}, \quad j = \mathrm{a,b} \tag{16}$$

With reference to method reported in the previous study [11], Z can be written as a superposition solution

$$Z(x,y) = Z_1(x,y) + Z_2(x,y) \tag{17}$$

where Z_1 and Z_2 attribute to the laser beam source in the nonhomogeneous boundary condition (Eq. (12)) and the moving interface in the nonhomogeneous governing equation (Eq. (11)), respectively. Converting the governing equation of Z_1 into a homogeneous Klein–Gordon equation and solving theoretically yield

$$\begin{aligned} Z_1(x,y) = {} & \frac{e^{\left(-\frac{Pe}{2}x\right)}}{\pi(l_1-l_2)} \int_{\omega=0}^{\infty} \frac{\cosh(\xi y)}{\xi^2(\xi\sinh\xi + Bi_u\cosh\xi)} \\ & \times \left\{ e^{\left(\frac{Pe}{2}l_1\right)} \left[\frac{Pe}{2}\cos(\omega(l_1-x)) + \omega\sin(\omega(l_1-x)) \right] \right. \\ & \left. - e^{\left(\frac{Pe}{2}l_2\right)} \left[\frac{Pe}{2}\cos(\omega(l_2-x)) + \omega\sin(\omega(l_2-x)) \right] \right\} d\omega \end{aligned} \tag{18}$$

where

$$\xi = \sqrt{\omega^2 + \frac{Pe^2}{4}} \tag{19}$$

In solving for the temperature Z_2 resulting from the heat absorption and heat release of the moving interfaces, the source-and-sink method is applied to first convert the problem to a nonhomogeneous Klein–Gordon equation. With proper expansion in Fourier series and integral combination, Z_2 can be solved and explicitly written for the four regions in the problem domain shown in Fig. 3 [12]

Region A:

$$\begin{aligned} & Z_2(x,y) \\ & = \sum_{n=1}^{\infty} C_n \left\{ -\frac{PeZ_p}{St} \int_{y_p}^{1} \left[e^{P_-(x-S_a(\eta))} - e^{P_-(x-S_b(\eta))} \right] H(p_n\eta)\,d\eta \right\} H(p_n y) \end{aligned} \tag{20}$$

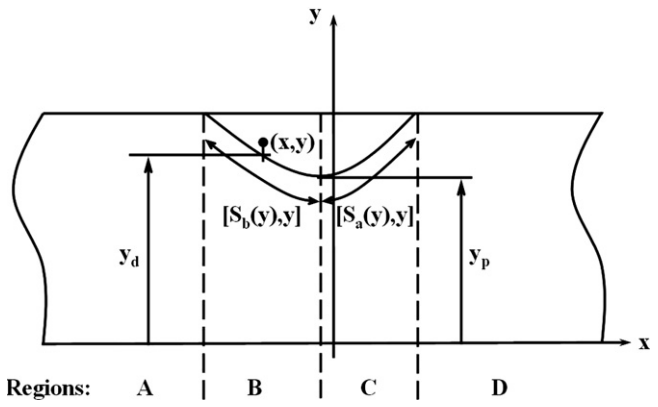

Fig. 3. Multiple regions in the moving dimensionless coordinates.

Region B:

$$\begin{aligned} & Z_2(x,y) \\ & = \sum_{n=1}^{\infty} C_n \left\{ -\frac{PeZ_p}{St} \left[\int_{y_p}^{1} e^{P_-(x-S_a(\eta))} H(p_n\eta)\,d\eta \right. \right. \\ & \left. \left. - \int_{y_p}^{y_d(x)} e^{P_-(x-S_b(\eta))} H(p_n\eta)\,d\eta - \int_{y_d(x)}^{1} e^{-P_+(x-S_b(\eta))} H(p_n\eta)\,d\eta \right] \right\} H(p_n y) \end{aligned} \tag{21}$$

Region C:

$$\begin{aligned} Z_2(x,y) = {} & \sum_{n=1}^{\infty} C_n \left\{ -\frac{PeZ_p}{St} \left[\int_{y_p}^{y_d(x)} e^{-P_+(x-S_a(\eta))} H(p_n\eta)\,d\eta \right. \right. \\ & + \int_{y_d(x)}^{1} e^{P_-(x-S_a(\eta))} H(p_n\eta)\,d\eta \\ & \left. \left. - \int_{y_p}^{1} e^{-P_+(x-S_b(\eta))} H(p_n\eta)\,d\eta \right] \right\} H(p_n y) \end{aligned} \tag{22}$$

Region D:

$$\begin{aligned} Z_2(x,y) = {} & \sum_{n=1}^{\infty} C_n \left\{ -\frac{PeZ_p}{St} \int_{y_p}^{1} \left[e^{-P_+(x-S_a(\eta))} \right. \right. \\ & \left. \left. - e^{-P_+(x-S_b(\eta))} \right] H(p_n\eta)\,d\eta \right\} H(p_n y) \end{aligned} \tag{23}$$

where

$$C_n = \frac{1}{2N(p_n)\sqrt{p_n^2 + \frac{Pe^2}{4}}} \tag{24}$$

$$N(p_n) = \frac{1}{2}\left[Bi_0 + \left(p_n^2 + Bi_0^2\right)\left(1 + \frac{Bi_u}{p_n^2 + Bi_u^2}\right) \right] \tag{25}$$

$$H(p_n y) = p_n \cos(p_n y) \tag{26}$$

and

$$P_{\pm} = \sqrt{p_n^2 + \frac{Pe^2}{4}} \pm \frac{Pe}{2} \tag{27}$$

The discrete eigenvalues p_n are obtained by solving the following expression:

$$\tan(p_n) = \frac{Bi_u}{p_n} \tag{28}$$

An iterative process based upon the concept of perturbation is employed to find the interface positions S_a and S_b. Eqs. (17)–(27) can be directly solved by numerical integration. The temperature profile $Z = Z_1 + Z_2$ in the moving coordinates will be used to determine the heating rate and cooling rate for the isothermal-transformation (IT) austenitization analysis and the continuous cooling transformation (CCT) pearitic/martensitic phase-transformation analysis, respectively. As a result, the enhanced material hardness is determined.

3. Experimental procedures

An experimental study on laser transformation hardening by a customized beam was conducted for validation of

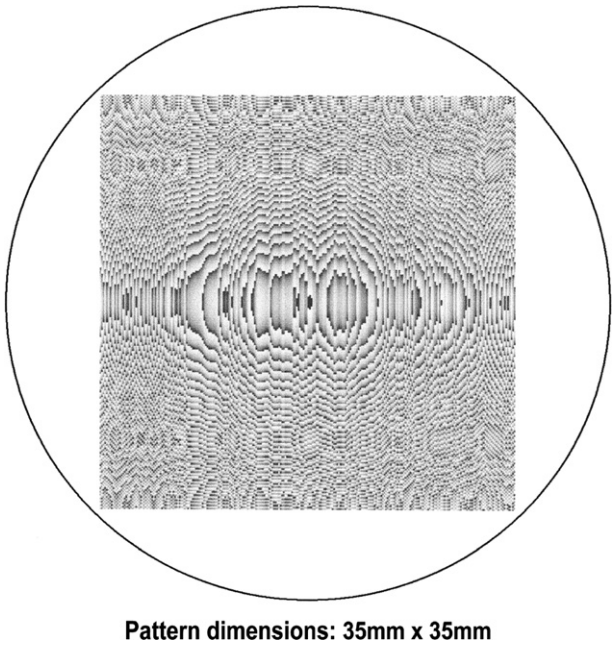

Fig. 4. Diffractive optical kinoform (DOK) used to produce a flat-top rectangular beam.

the theoretical model developed. The sample was made of AISI 1050 steel having a chemical composition of C(0.47–0.55), Mn(0.6–0.9), P(max 0.04), and S(max 0.05). The sample was machined to a 300 mm × 25 mm × 13 mm rectangular bar. The test surface was ground with 220-grit SiC paper and then sandblasted with 200-grit SiO_2. Finally, a graphite dag layer was coated on the test surface. A laser power meter was used to measure the laser absorptivity of the coated surface and it was found to be about 60%.

A high-power CO_2 laser was regulated to generate 0.8-kW output. The original Gaussian spot beam was customized to a flat-top rectangular beam by means of a diffractive optical kinoform (DOK). The DOK was a computer generated holographic element with specially designed array cell pattern as shown in Fig. 4. The customized beam size was 15 mm × 2 mm and the beam power was specified to be 60% of the incident beam. The laser transformation hardening experiment was set up as illustrated in Fig. 1. The steel sample bar was insulated on all sides, except the upper test surface. The feed rate was controlled at constant 0.83 mm s^{-1} (50 mm min^{-1}) for the laser beam to scan along the entire 300 mm span of the steel sample. The hardening effect was measured by a microindentation hardness tester (model BUEHLER 1600-6301).

4. Results and discussion

In order to avoid any confusion, all the temperatures mentioned in the remaining discussion are measured above a common reference of absolute temperature at 273 K. The material properties of AISI 1050 steel and the laser transformation hardening test parameters used in both theoretical analysis and experimental test are listed in Table 1.

Table 1
Properties of AISI 1050 steel specimen and laser transformation hardening test parameters

Material properties	
ρ (kg m^{-3})	7817
k (W m^{-1} K^{-1})	30
c (kJ kg^{-1} K^{-1})	0.46
L (kJ kg^{-1})	83.6
T_p (°C)	770
Test parameters	
u (mm)	13
q_0 (kW)	0.8
DOK efficiency	60%
Surface absorption	60%
q (kW) calculated	0.288
l (mm)	2
w (mm)	15
V (mm s^{-1})	0.83
h_u (W m^{-2} K^{-1})	180
h_0 (W m^{-2} K^{-1})	0
Dimensionless parameters	
Pe	1.29
St	4.1
Bi_u	0.078
Bi_0	0
Z_m	1.16
l_1	0.0769
l_2	−0.0769

4.1. Theoretical results

In the theoretical analysis, solving the dimensionless Eqs. (17)–(27) followed by a conversion to dimensional results yielded the temperature profiles as plotted in Fig. 5. The case depth of the hardened material could be determined from the temperature profiles. Although the material at a depth of 650 μm exceeded the phase-transformation temperature T_p (AC_3) of 770 °C, the material would be hardly transformed to the austenitic phase for subsequent pearlitic/martensitic transformation because

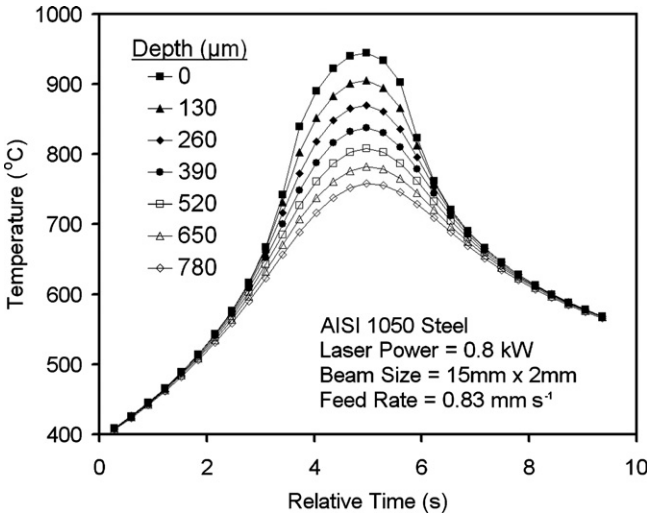

Fig. 5. Heating and cooling temperature profiles at various depth.

the heating process above 770 °C last for only a short instant. With reference to the IT diagram for rapid austenitization, complete austenitization (100% austenite) would be formed at a depth of 260 μm where the material was heated above 770 °C with a mean temperature of 833 °C for 2 s [14,15]. Therefore, the predicted case depth was 260 μm. The material just below the case depth did not undergo complete austenitization due to insufficient heating time. Thus, the subsequent cooling process, depending on the cooling rate, could only produce partial martensite or pearlite that formed a transitional zone with a hardness lower than that of the upper hardened zone.

The temperature profiles shown in Fig. 5 could also be used to predict the hardness. The temperature profiles of the material within the case depth, labeled by solid squares, solid triangles, and solid diamonds, were very close during the cooling process below T_p of 770 °C. The cooling rate at 770 °C was 130 °C s^{-1} and gradually decreased with time. The average cooling rate between 770 °C and 600 °C was 67.4 °C s^{-1}. With reference to the CCT diagram [16], all the austenite would be transformed to pearlite without any formation of martensite. The predicted hardness within the case depth of 260 μm was 370 HV.

4.2. Experimental results

In the experimental study, detailed hardness measurements were conducted for the material at mid-length of the steel sample. The surface hardness profile across the sample width, i.e. the z'' direction, was measured. The measurements presented in Fig. 6 showed a uniform hardness distribution within the irradiated area, $-7.5\text{ mm} \leqslant z'' \leqslant 7.5\text{ mm}$, with a mean value of 355 HV. The results validated the simplification of the problem to a two-dimensional model as the majority hardening effect was independent of z''. The hardness values at both ends, $z'' < -7.5$ mm and $z'' > 7.5$ mm, were relatively low because the heat dissipation in the z'' direction diminished the heating effect for austenitization. In comparison with the theoretical prediction, the predicted hardness of 370 HV deviated from the mean measurement of 355 HV by 4.2%.

The sample was cut in the middle for more hardness measurements along the depth of the centerline. The measurements are presented in Fig. 7. At a depth greater than 240 μm, the hardness was around 280 HV showing no noticeable hardening effect. From 240 to 180 μm depth, an obvious increase in hardness occurred in this transitional zone. Additionally, as illustrated in Fig. 8 showing the micrograph of the cross-sectional view, the case depth could vary between 190 μm and 320 μm. Such variation could be caused by variation in laser absorption due to nonuniform properties of the surface prepared by grinding, sandblasting, and coating of laser absorbing layer. As a result, the theoretically predicted case depth of 260 μm was consistent with the experimental measurements. Fig. 9 clearly shows the interface between the austenitic and pearlitic microstructures.

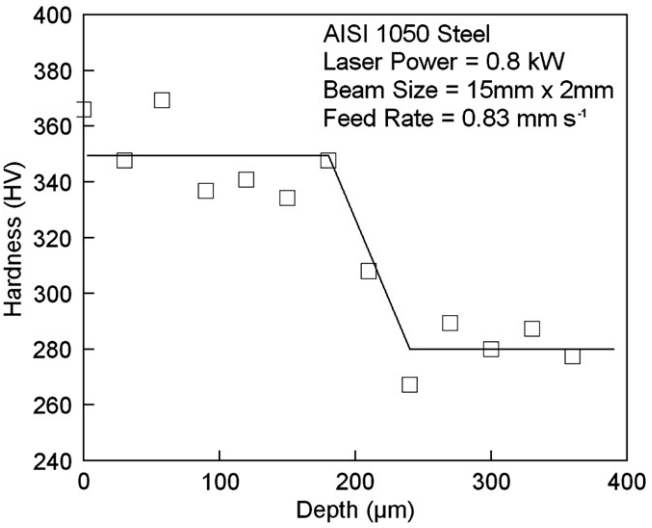

Fig. 7. Hardness versus depth.

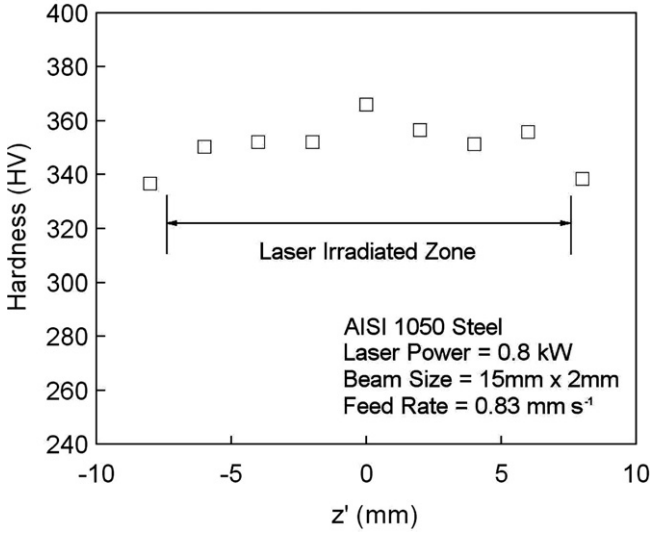

Fig. 6. Surface hardness after laser transformation hardening.

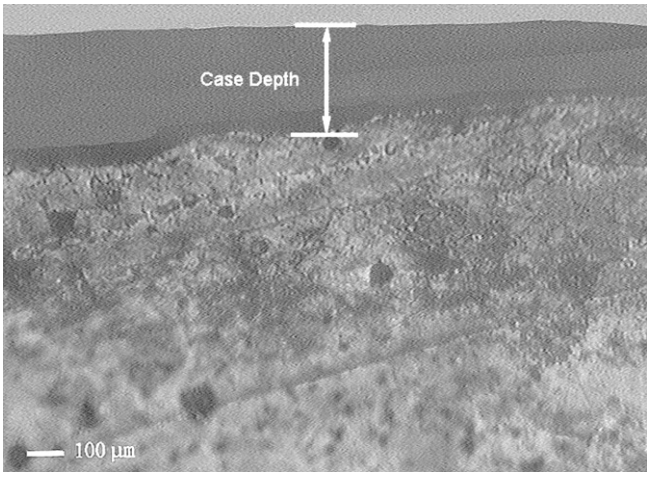

Fig. 8. Micrograph showing the case depth of hardened material.

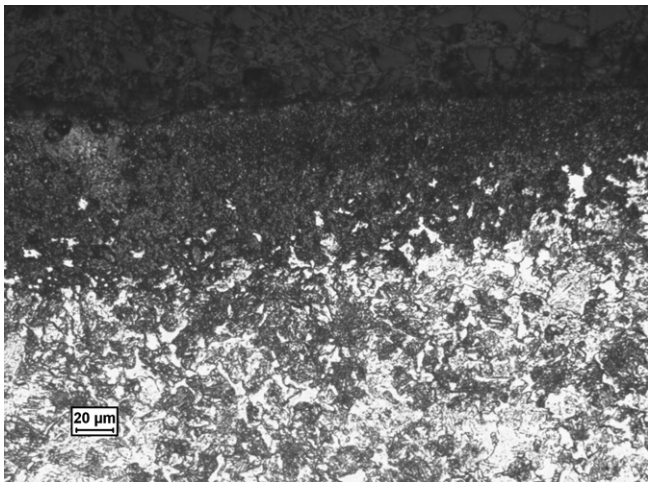

Fig. 9. High-resolution micrograph of the phase-change interface.

The hardness measurements shown in Fig. 7 were also compared with the theoretical predictions. The maximum, minimum, and mean of the microhardness values measured between 0 and 180 μm depth were 370 HV, 334 HV, and 349 HV, respectively. The predicted hardness of 370 HV just fell within the measurement range and deviated from the mean measurement of 349 HV by 6.0%. A reasonable agreement between the theoretical and experimental results was obtained for the laser transformation hardening effects in terms of case depth and hardness. Although the model validation was done for pearlitic transformation, it implied that the theoretical model could be used for martensitic transformation because the two phase-transformation mechanisms are basically the same.

For the process parameters used in the above illustration, only pearlite was formed without any martensite in the hardened zone because of the low cooling rate. Thus, the hardness was not increased by a significant amount. The hardening process could be improved by increasing the feed rate as well as the laser power. Using the exact solution developed in this study, it was found that a 1.5-kW laser source with a feed rate of $3.33\ \mathrm{mm\ s^{-1}}$ ($200\ \mathrm{mm\ min^{-1}}$) could yield surface material cooling from 770 °C to 250 °C at a mean rate of $130\ ^{\circ}\mathrm{C\ s^{-1}}$. The consequent hardening effect would be 100% martensitic transformation for the material within a case depth of 130 μm with a surface hardness of 820 HV.

5. Conclusion

This paper presents a derivation of an exact solution for modeling the moving-interface heat transfer in a laser transformation hardening process. The solution is illustrated for a customized laser beam with a flat-top rectangular configuration. The techniques used to solve a Klein–Gordon equation with expansion in Fourier series and integral combination were employed in the derivation. The theoretical predictions in terms of case depth and increased material hardness agreed well with the experimental results. Besides laser transformation hardening, the exact solution can be applied to other laser heat treatment processes involving moving phase-change interfaces, such as glazing, sealing, alloying, and cladding.

Acknowledgments

The work described in this paper was fully supported by a grant from the Research Grants Council of the Hong Kong Special Administrative Region, China (Project No. HKU 1008/01E) and a grant from the University Research Grants (No. 10206014) of the University of Hong Kong.

References

[1] L.J. Yang, S. Jana, S.C. Tam, The effects of overlapping runs in the laser-transformation hardening of tool-steel specimens, J. Mater. Process. Technol. 23 (1990) 133–147.
[2] A. Primartomo, K. Williams, I.A. Ashcroft, Laser transformation hardening using customised laser beam intensity profiles, in: Proceedings of the First Pacific International Conference on Application of Lasers and Optics, LMP-LSIII, 2004, pp. 29–34.
[3] R. Komanduri, Z.B. Hou, Thermal analysis of the laser surface transformation hardening process, Int. J. Heat Mass Transfer 44 (2001) 2845–2862.
[4] R. Brockmann, K. Dickmann, P. Geshev, K.-J. Matthes, Calculation of temperature field in a thin moving sheet heated with laser beam, Int. J. Heat Mass Transfer 46 (2003) 717–723.
[5] H.G. Landau, Heat conduction in a melting solid, Quart. Appl. Math. 8 (1950) 81–94.
[6] F. Jackson, Moving heat sources with change of phase, ASME J. Heat Transfer 87 (1965) 329–332.
[7] C.K. Hsieh, Exact solution of Stefan problems for a heat front moving at constant velocity in a quasi-steady state, Int. J. Heat Mass Transfer 38 (1995) 71–79.
[8] C.K. Hsieh, Exact solution of Stefan problems related to a moving line heat source in a quasi-stationary state, ASME J. Heat Transfer 117 (1995) 1076–1079.
[9] C.K. Hsieh, C.-Y. Choi, Solution of one- and two-phase melting and solidification problems imposed with constant or time-variant temperature and flux boundary conditions, ASME J. Heat Transfer 114 (1992) 524–528.
[10] C.K. Hsieh, C.-Y. Choi, A general analysis of phase change energy storage for solar energy applications, ASME J. Solar Energy Eng. 114 (1992) 203–211.
[11] C.K. Hsieh, M. Leung, Phase change in a cylinder and a cylindrical shell heated with an axisymmetric front moving in the axial direction, ASME J. Heat Transfer 123 (2001) 476–484.
[12] M. Leung, Phase-change heat transfer in laser transformation hardening by moving Gaussian rectangular heat source, J. Phys. D: Appl. Phys. 34 (2001) 3434–3441.
[13] P.D. Patel, Interface condition in heat conduction problems with change of phase, AIAA J. 6 (1968) 2454–2456.
[14] C.R. Brooks, Austenitization of Steels, Principles of the Heat Treatment of Plain Carbon and Low Alloy Steels, ASM International, 1996, pp. 205–234 (Chapter 6).
[15] J. Hershberger, O.O. Ajayi, J. Zhang, H. Yoon, G.R. Fenske, Formation of austenite during scuffing failure of SAE 4340 steel, Wear 256 (2004) 159–167.
[16] G.F. Vander Voort, Atlas of Time–Temperature Diagrams for Irons and Steels, ASM International, 1991.